4 Problems of actual-value measurement and vector orientation

This chapter aims to explain principles of the actual-value measurement, to highlight its problems and to answer some related questions of the field orientation.

The current measurement technique influences decisively the controller design and thus also the dynamic characteristic of the inner current control loop, which in turn is the prerequisite for the superimposed speed control. So the actual-value measurement is an important interface of every drive control system which must be taken into account very carefully for the controller design.

Similarly, for the design of the speed control loop the speed measuring is an important issue to consider. Either an incremental encoder or a resolver can be used to measure the speed. Also the alternative possibility of sensorless capture of the speed will be discussed, and possible ways to solve this problem will be shown.

The second problem of this chapter is the field orientation, which is very closely connected to the speed measurement. Field orientation means namely,

1. that the field angle ϑ_s and respectively the location of the field coordinate system (*dq*- coordinates) must be calculated, and
2. that the un-measurable rotor flux, which will be used for calculating the rotor frequency or the slip and therefore also the field angle ϑ_s, has to be estimated. The estimated value of the rotor flux can be used as actual value in the flux control loop, which is – for example – of decisive importance for field-weakening operation.

The estimation of the rotor flux, which can be realized either by flux models or by flux observers, and the calculation of the field angle require actual values of current and speed.

4.1 Acquisition of the current

The measurement of the currents can be performed as shown in the figure 1.3. Depending on the coordinate system the inner current control loop is realized in – field synchronous or stator-fixed – actual values $i_{s\alpha}$, $i_{s\beta}$ or i_{sd}, i_{sq} are obtained after the transformation of the measured phase currents i_{su} and i_{sv}. What could not be indicated in this figure are:

1. The technical realization of the measurement and
2. the fact, that *for the current control only the instantaneous value of the fundamental wave is relevant*.

From the technical view, two possibilities to measure the currents exist:

1. The most advanced technique is the measurement of instantaneous values using A/D converters (ADC: Analog to Digital Converter) and
2. The integrating measurement using V/f converters (VFC: Voltage to Frequency Converter).

a) Measurement of instantaneous values using an ADC

This method is frequently applied because of the simplicity of its technical realization and the possibility of a high resolution. The inherent current harmonics have to be suppressed, for example by an additional filter. This however, would result in an additional delay of the measured values. This delay is unwanted, and therefore has to be avoided if possible, to maintain the dynamics of the current control loop, particularly for the new current controller designs in chapter 5.

The *time instant of the current measuring* plays a decisive role for the exact acquisition of the fundamental wave and for the elimination of the pulse frequent harmonics. To achieve this, the measuring instant must be exactly placed in the middle of the zero vector times T_0 or T_7 (using the modulation algorithm in the chapter 2). The figure 4.1 explains the facts.

This measuring strategy has the advantage that the otherwise necessary filter becomes superfluous and the delay connected to it disappears. The obvious disadvantage is, particularly under transient conditions, that the time instant of the measurement sampling will shift (start-up, reversing, field weakening etc.), because the values of the zero vector time T_0 or T_7 are not constant, but depend on the operating state of the motor. The measurement sampling instants, illustrated in the figure 4.1, correspond to the output sequence of $\mathbf{u}_s$ using the time pattern in the figure 2.9a.

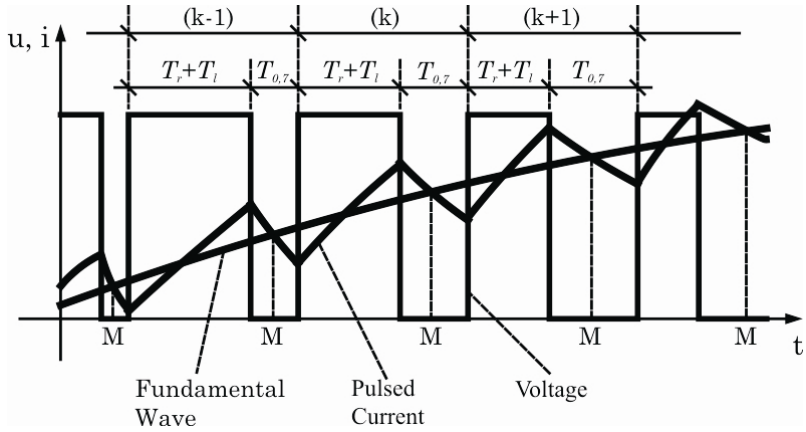

Fig. 4.1 The current measurement sampling instants (*M*) using an A/D converter

The mentioned disadvantage of the shifting sampling instant disappears if the output sequence of the time pattern in figure 2.9b is used. The sampling instant will be exactly in the middle of T_7 and consequently, the pulse and the control sampling frequency will exactly coincide (figure 2.9b).

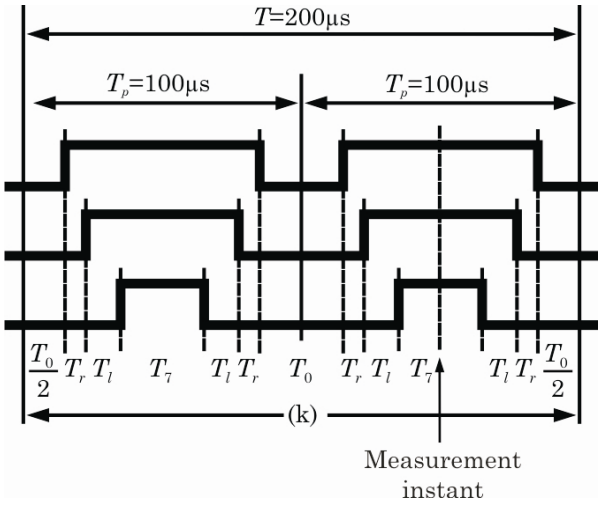

Fig. 4.2 A strict synchronization between pulse period and measurement sampling with sampling in the center of zero vector times

With the tendency toward higher pulse frequencies, the pulse frequency can, however, be a multiple of the sampling frequency. The measurement sampling must always be located either in the center of the last zero vector

time T_7 or at the starting points of the sampling periods of the control system. The outlined principle for the realization of the current measurement clarifies the demand for a strict synchronization between pulse periods and measurement sampling which must already be thought through at the hardware design stage. The figure 4.2 presents an example with 10kHz pulse frequency and 5kHz sampling frequency.

b) The integrating measurement using a VFC

This category also includes the method of analog integration with subsequent A/D conversion. The measured signal is converted into a pulse sequence with a frequency which is directly proportional to its amplitude. This pulse sequence is applied to an up/down counter whose counting direction is switched over according to the sign of the measured signal. The impulses are counted over one sampling period. Because of the integrating behavior there is no need for special measures to suppress pulse frequent harmonics. However, the result of the integration does not represent the instantaneous values of the fundamental, which are needed by the control system. They may be back-propagated using an interpolation filter, for example of second order as in equation 4.1.

$$\mathbf{i}_s(k) = 1{,}83\,\bar{\mathbf{i}}_s(k) - 1{,}16\,\bar{\mathbf{i}}_s(k-1) + 0{,}33\,\bar{\mathbf{i}}_s(k-2) \tag{4.1}$$

k: 0, 1, 2, ... , ∞; $\bar{\mathbf{i}}_s$: Integrated value

The interpolation filter may be fed with either the phase currents i_{su}, i_{sv} directly or the current components in dq or $\alpha\beta$ coordinates. That means, the back-propagation of the instantaneous values of the fundamental happens before or after processing equations (1.6) and (1.7). The results would show, depending on the sensor resolution largely corresponding feedbacks and actual motor currents, with the restriction that sampling-frequent oscillations cannot be followed. Since only actually measured mean average values of the currents are available, this fact requires special measures for the design of the current controller. Chapter 5 will more deeply deal with these issues.

4.2 Acquisition of the speed

The speed is commonly measured either with a resolver or with an incremental encoder. Because of the pulse counting when using an incremental encoder and the averaging of the speed, over several sampling periods by differentiating the position angle with resolver, the measurement has an integrating characteristic and does not show the

instantaneous value of the speed. Similar to the above discussed back-propagation for the current feedback, an interpolation of the measured values might be used to reconstruct the speed instantaneous values (here with filter of first order).

$$\omega(k) = 1{,}5\bar{\omega}(k) - 0{,}5\bar{\omega}(k-1) \tag{4.2}$$

$\bar{\omega}$= Integrated actual feedback value

a) Measurement of speed using an incremental encoder (IE)

As is well known, the IE delivers two by 90^0 phase-shifted signals A and B (fig. 4.3) in the form of square pulses, where the impulse number per revolution is given by the construction of the encoder device. The additional channel zero provides once per revolution a zero reference impulse, which is normally congruent with the edges of one of the channels A or B. By measuring of the impulse frequency f_M the speed n can be determined.

$$n = \frac{60\, f_M}{z_{IE}} = [rpm] \tag{4.3}$$

$f_M =$ Frequency [in Hz] of the impulse sequence

$z_{IE} =$ Number of impulses per revolution

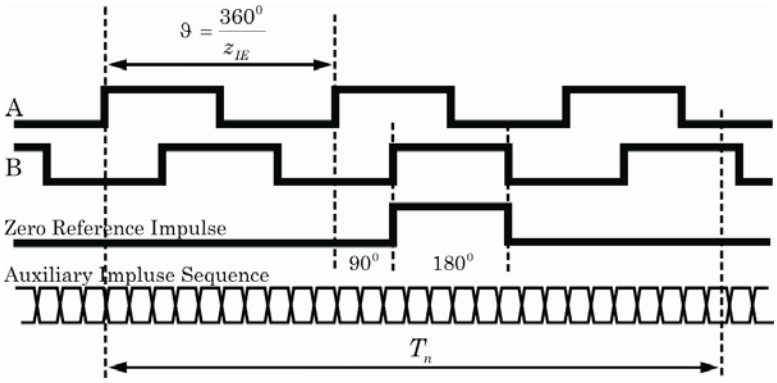

Fig. 4.3 Use of an incremental encoder (IE) to measure the speed

By evaluation of the phase relationship between the signals A and B the direction of rotation can be found. For a given IE and thus defined f_M, the maximal measurable speed n_{max} can be calculated by equation (4.3). Or conversely, with predefined motor and maximal speed n_{max}, the maximal necessary f_M can also be calculated by (4.3).

If the rotor position is described by ϑ, and the sampling period of the speed control by T_n, then the frequency measurement transforms into a counting of the impulses A or B within T_n following the equation:

$$n = \frac{\vartheta(k) - \vartheta(k-1)}{T_n} \tag{4.4}$$

k = 0, 1, 2, ... , ∞ = Sampling time instants

The impulse counting alone does not suffice for a precise measurement at very low-speeds, and here has to be amended by a time measurement where the time for the passing of a certain angular sector is measured with the help of an additional higher-frequent impulse sequence (fig. 4.3). From the equation (4.4) the speed can be obtained as follows:

$$n = \frac{\vartheta}{t(k) - t(k-1)} \text{ with } \vartheta = \frac{360^0}{z_{IE}} = \frac{1 \text{ rev}}{z_{IE}} \tag{4.5}$$

The measurement resolution can be found by generalization of the equations (4.4), (4.5). Equation (4.4) can be rewritten as follows:

$$n = \frac{60}{z_{IE}\, T_n} n_{IE} \quad \text{in } \left[\min^{-1}\right] \tag{4.6}$$

n_{IE} = Number of impulses counted during T_n

The resolution of the speed measurement, using pure impulse counting, can be obtained after derivation of equation (4.6).

$$\frac{dn}{dn_{IE}} = \frac{60}{z_{IE}\, T_n} \text{ or } \Delta n \approx \frac{60}{z_{IE}\, T_n} \Delta n_{IE} \tag{4.7}$$

With, for example,

$\Delta n_{IE} = 1$ (Only 1 impulse is counted during T_n)

$z_{IE} = 1024$ (IE produces 1024 pulses per revolution)

$T_n = 1ms$ (Sampling period)

a resolution of $\Delta n \approx$ 58,6 min^{-1} is obtained. With the help of impulse quadruplication this result can be improved essentially. The equation (4.5) for period measurement can be rewritten as follows:

$$n = \frac{60}{z_{IE}} \frac{1}{\tau} \quad \text{in } \left[\min^{-1}\right] \tag{4.8}$$

τ = in [s] measured time for the passed angle sector $360^0/z_{IE}$

The first derivation of equation (4.8) delivers:

$$\frac{dn}{d\tau} = -\frac{60}{z_{IE}\, \tau^2} \text{ or } \Delta n \approx -\frac{60}{z_{IE}\, \tau^2} \Delta\tau \tag{4.9}$$

Using a 20 MHz impulse sequence (time resolution $\Delta\tau$ = 50 nsec) and a 10-bit counter (maximal measurable time τ = 2^{10}×50 ns = 51,2 µs) a resolution of $\Delta n \approx$ 1,1176 rpm can be obtained for very low-speeds.

Another possibility to reach a high-resolution result for low-speeds is to use an IE with approximately sinusoidal output signals A and B (fig. 4.4).

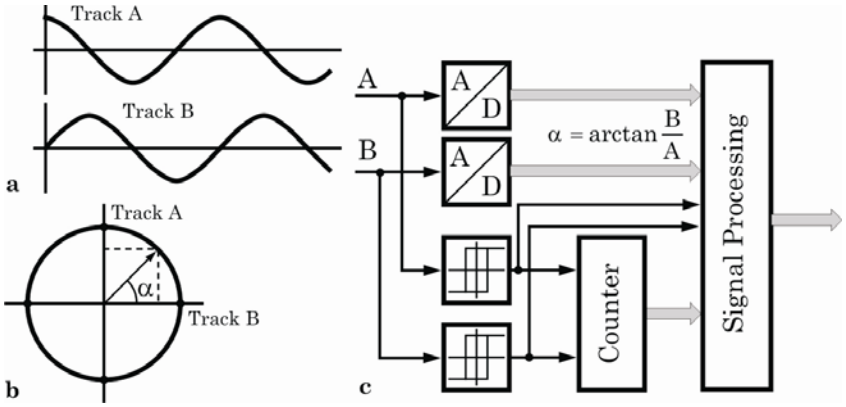

Fig. 4.4 Use of an incremental encoder with sinusoidal output signals for speed measuring

After zero-crossing detection the signals can be processed exactly as in the case of an usual IE. With two additional A/D converters and high-frequency sampling within a signal period, the speed is obtained from:

$$n = \frac{d\alpha}{dt} = \frac{d}{dt}\left(\arctan\frac{B}{A}\right) \tag{4.10}$$

b) Measurement of speed using a resolver

The construction of a resolver is shown in the figure 4.5a. The resolver consists of two parts. The mobile part (the rotor) is fixed to the motor shaft and contains the primary excitation winding, fed by a rotating transformer with an excitation signal of approx. 2...10 kHz. The static part (the stator) contains two secondary (sine, cosine) windings, which are mechanically displaced at 90 deg against each other.

In principle two methods for processing the resolver signals exist. The first one is called angle comparison (fig. 4.6a) and is implemented in integrated circuits like AD2S82 or AD2S90[1)]. The angle comparison is carried out with the help of a multiplier (RM: Ratio Multiplier) at the input, which calculates an angle error. After the multiplier (fig. 4.5), the following results are obtained at the outputs of sine/cosine channels:

$$t_c\, u_0 \sin(\omega t)\sin\vartheta\cos\vartheta_M \quad \text{and} \quad t_c\, u_0 \sin(\omega t)\cos\vartheta\sin\vartheta_M \tag{4.11}$$

[1)] from the firm Analog Devices

Substracting the signals of the equation (4.11) from each other yields the error signal:

$$\begin{aligned}\Delta\vartheta &= t_c\, u_0 \sin(\omega t)\left(\sin\vartheta\, \cos\vartheta_M - \cos\vartheta\, \sin\vartheta_M\right)\\ &= t_c\, u_0 \sin(\omega t)\sin\left(\vartheta - \vartheta_M\right)\end{aligned} \tag{4.12}$$

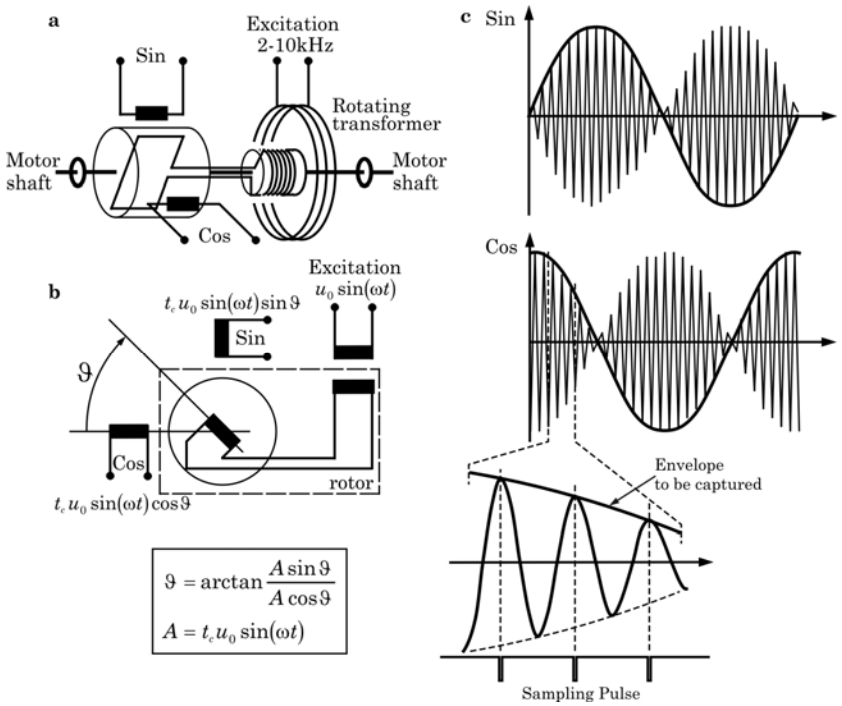

Fig. 4.5 Principle mechanical (**a**) and schematic (**b**) construction of the resolver with its output signals (**c**). t_c: transmission coefficient; u_0: amplitude of excitation signal

According to equation (4.12) the error $\Delta\vartheta$ disappears if the difference $\vartheta - \vartheta_M$ becomes zero. To achieve this, the error signal is fed via a phase sensitive detector (PSD) to an integrator or a PI controller whose output controls a voltage-controlled oscillator (VCO). A up/down counter (UDC) counts the impulses coming from the output of the VCO, in which the counting direction of the UDC depends on the sign of the error signal. This way the phase error will be eliminated with the help of an integrator or a PI controller. The dynamics of the measurement depends on the dynamics of the control loop which poses a considerable disadvantage for the complete system.

The measuring dynamics can be increased significantly if the envelope of the resolver signals (see figure 4.5c) can be captured directly, i.e.

always at the peak value of the curve. With the help of two A/D converters (fig. 4.6b) this can be realized easily provided a *strict synchronization between the measurement sampling, control and modulation,* is observed and taken care of already in the hardware design. Furthermore it has to be considered that the resolver signals are susceptive to noise and distortions through the transmission paths between motor and electronics which may result into loss of the original synchronization and a signal correction (usually by software) becomes necessary.

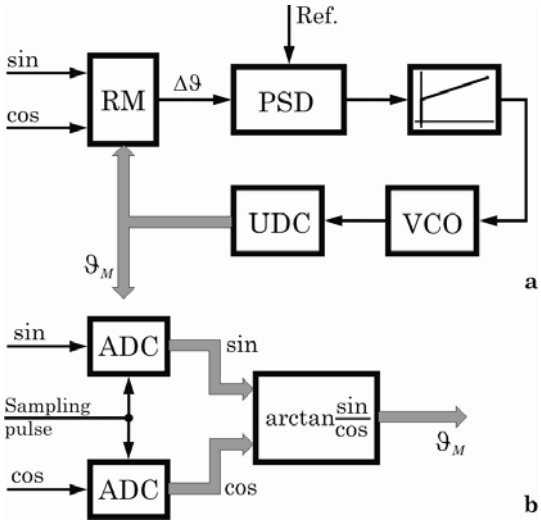

Fig. 4.6 Methods for evaluation of resolver signals: Angle comparison (**a**) and signal sampling with two A/D converters (**b**)

From the relation:

$$\vartheta = \arctan\frac{x}{y} \quad \text{with} \quad x = \sin\vartheta;\ y = \cos\vartheta$$

the total differential of ϑ can be derived easily:

$$\mathrm{d}\vartheta = y\,\mathrm{d}x - x\,\mathrm{d}y \tag{4.13}$$

and:

$$\Delta\vartheta \approx y\,\Delta x - x\,\Delta y \tag{4.14}$$

With $\Delta x = \Delta y = 2^{-z_{ADC}}$, in which z_{ADC} is the resolution of the A/D converter, the corresponding resolution of the measured angle can be assessed.

Considering that the derivatives dx/dt und dy/dt can assume values independent of z_{ADC} at the actual time, and from the relationship for the speed n:

$$n = \frac{60}{2\pi z_p}\omega = \frac{60}{2\pi z_p}\frac{\mathrm{d}\vartheta}{\mathrm{d}t}\ \left[\mathrm{min}^{-1}\right] \tag{4.15}$$

the total differential for n can be derived after some conversions:

$$\mathrm{d}n = n\left(x\,\mathrm{d}x + y\,\mathrm{d}y\right) \tag{4.16}$$

From (4.16) results:

$$\Delta n \approx n\left(x\Delta x + y\Delta y\right) \tag{4.17}$$

With the equation (4.17) also the speed resolution, depending on the operating point, can be assessed using $\Delta x = \Delta y = 2^{-z_{ADC}}$.

Because the resolver provides the absolute position information, it can be used advantageously in synchronous drives. In addition, the resolver is robust against external influences like high temperatures or magnetic interference fields. With respect to the measuring precision the resolver, however, cannot achieve the high resolution of the IE with analog or sinusoidal output signals.

4.3 Possibilities for sensor-less acquisition of the speed

The idea to save the speed sensor, and to reduce not only the costs but also to increase the reliability, because mechanical parts and the sensitive galvanic connection between sensor and actuator are omitted, was the motivation for numerous research in the last two decades. In principle the developed methods can be divided into three groups:

1. Stator flux orientated methods like Direct Torque Control (DTC), Natural Field Orientation (NFO).
2. Rotor flux orientated methods, following the principle of a Kalman Filter (KF) or a Model Reference Adaptive System (MRAS).
3. Methods which use machine specific effects (unbalance, slots on stator and rotor side etc.).

With respect to the theoretical approaches, the solutions to this problem are very different and partly based on special effects so that not all of them can be discussed in the context of this chapter. Because of the many advantages compared to the stator flux orientation, this chapter exclusively deals with the rotor or pole flux orientated drive systems which are very widespread in practice. Consistently only examples of rotor flux orientated methods will be discussed because the methods to be selected, must be

suited for integration into the overall control system. The methods based on the use of machine specific effects can also be used very well in systems controlled with field orientation.

In the area of higher frequencies the speed sensor-less operation works without problems for all methods in the case of an asynchronous drive. The critical area is the area around standstill. The results published in the last decade have led to the conclusion that *zero stator frequency in the case of the IM represents a virtually not observable point and therefore cannot* be controlled correctly *with conventional methods like DTC, NFO, KF, and MRAS*. At set points near zero speed and under influence of a strong load, the rotor can always drift away without the system reacting to it. Thereat the rotor flux vector rotation stops. This is primarily based on the fact, that the magnetization of the slowly rotating rotor of the IM can be easily changed by the (almost) still standing rotor flux vector. Only if the mechanical frequency of motion reaches a certain limit (approximately the slip frequency) and thus the magnetic reversal is no longer possible, the speed can be calculated correctly again. *A clean reversal across the speed zero is always possible, though*. Use of the above mentioned methods, including the already commercialized DTC, always implies theoretically unsolidated detours.

In the case of a PMSM drive, the standstill is less critical because the pole flux is built up permanently. Therefore a magnetic reversal process can not take place, and the moving pole delivers information for the estimation already at low-speeds. Two problems must be solved here:

- The *initial position of the pole flux* must be identified: For the case of an asymmetric rotor build-up (e.g. salient pole machines or full pole machines with only few magnets on the rotor surface), many useable approaches can be found in the literature. The question is still relatively open for machines with exclusive full pole quality (i.e. the magnets are assembled in a larger number, and thus divided up finer) on the rotor surface thanks to the high energy density and the improved construction.
- The development of a *method for the speed sensor-less control* of the drive. The variety of the useable methods is similar as in the case of the IM.

The methods based on the use of the machine specific effects are best suitable both for IM and for PMSM. The unbalances in the mechanical construction and the slots on stator and rotor side are mirrored in the harmonics of the stator currents independent of their fundamental frequency.

In this chapter only two application examples are presented for the speed sensor-less control of the IM and PMSM. For the IM the control system has the principle structure of figure 4.7. It can still be recognized

that the structure of figure 4.7 also applies to the case of the PMSM drive if the flux controller is dropped and the corresponding algorithm is implemented in the context of the "speed adaptive observer".

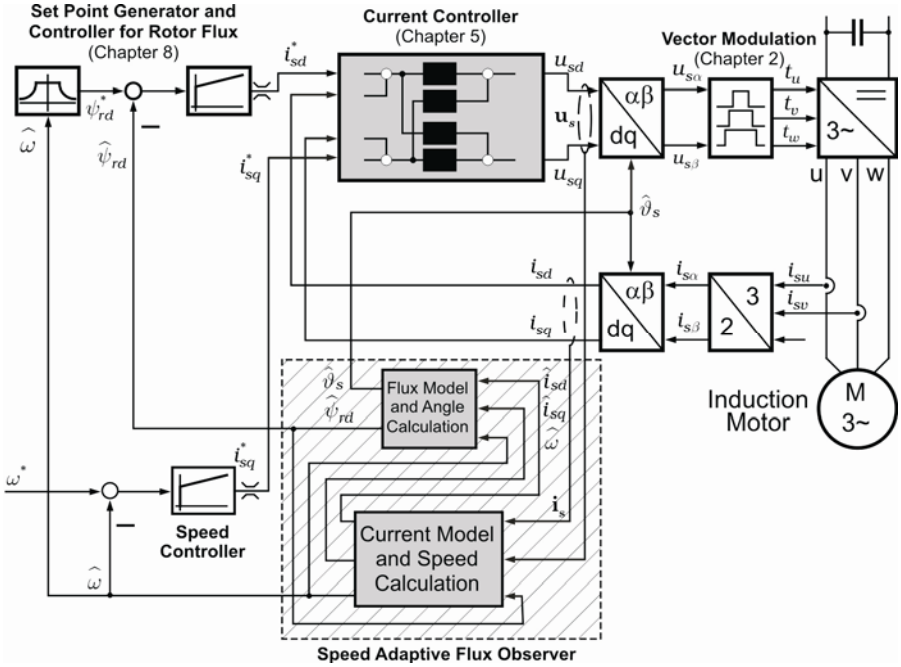

Fig. 4.7 General structure of speed sensor-less and rotor flux orientated control of an IM drive in *dq* coordinates

4.3.1 Example for the speed sensor-less control of an IM drive

As is well known, the IM can be completely described by the state model (3.41) (cf. section 3.2) electrically. If we start from the assumption that the machine parameters are time-invariant, then only in the equation (3.41) depends on the speed and must be updated on-line with *a measured or estimated speed*. The estimated quantities are denoted with an index „∧“ in the following.

With the model (3.41) a Luenberger observer can be used to reconstruct the state vector (fig. 4.8a).

$$\frac{d\hat{\mathbf{x}}}{dt} = \hat{\mathbf{A}}\hat{\mathbf{x}} + \mathbf{B}\mathbf{u}_\mathbf{s} + \mathbf{K}\left(\mathbf{i}_\mathbf{s} - \hat{\mathbf{i}}_\mathbf{s}\right) \tag{4.18}$$

$\mathbf{K}$ = Correction matrix

For the case of measured speed numerous approaches to design **K** (e.g. with the help of pole assignment) have been presented. The observer (4.18) then delivers only estimates for the not measurable rotor flux. If the speed, regarded as a system parameter in this model, shall be estimated together with the state quantities, the structure must be extended like shown in figure 4.8b.

Using the definition of the state error **e**:

$$\mathbf{e} = \mathbf{x} - \hat{\mathbf{x}} \tag{4.19}$$

the following error state equation is obtained after subtracting (3.41) and (4.18):

$$\frac{d\mathbf{e}}{dt} = (\mathbf{A} + \mathbf{KC})\mathbf{e} + \Delta\mathbf{A}\hat{\mathbf{x}} \tag{4.20}$$

with:

$$\Delta\mathbf{A} = \mathbf{A} - \hat{\mathbf{A}} = \left[\begin{array}{c|c} \mathbf{0} & \Delta\omega\dfrac{1-\sigma}{\sigma}\mathbf{J} \\ \hline \mathbf{0} & -\Delta\omega\,\mathbf{J} \end{array}\right] \tag{4.21}$$

$$\mathbf{J} = \begin{bmatrix} 0 & 1 \\ -1 & 0 \end{bmatrix}; \Delta\omega = \omega - \hat{\omega} = \text{Parameter error}$$

The state estimation techniques using a speed adaptation like in figure 4.8b, are part of the category of methods with model reference adaptive systems (MRAS) in which the motor (the process) plays the role of the reference model.

Because of the nonlinear (process) behavior the stability aspect must be included at the design of such systems from the beginning (cf. [Isermann 1988], chapter 22.3). The stability proof can be carried out either using Popov's method of hyper stability (e.g. [Tajima 1993]) or the direct method of Ljapunov (e.g. [Kubota 1993 and 1994]). The latter will be used in the following.

The Ljapunov function V for the error equation (4.20) is chosen to contain both the state error **e** and the parameter error $\Delta\omega$.

$$V = \mathbf{e}^T\,\mathbf{e} + \frac{[\Delta\omega]^2}{\lambda} \tag{4.22}$$

λ = Positive constant

The first derivation of V yields:

$$\begin{aligned} \frac{dV}{dt} = \mathbf{e}^T &\left[(\mathbf{A} + \mathbf{KC})^T + (\mathbf{A} + \mathbf{KC})\right]\mathbf{e} \\ &- 2\Delta\omega\left(\tilde{i}_{s\alpha}\,\hat{\psi}'_{r\beta} - \tilde{i}_{s\beta}\,\hat{\psi}'_{r\alpha}\right)\frac{1-\sigma}{\sigma} + 2\Delta\omega\frac{d\hat{\omega}}{dt}\frac{1}{\lambda} \end{aligned} \tag{4.23}$$

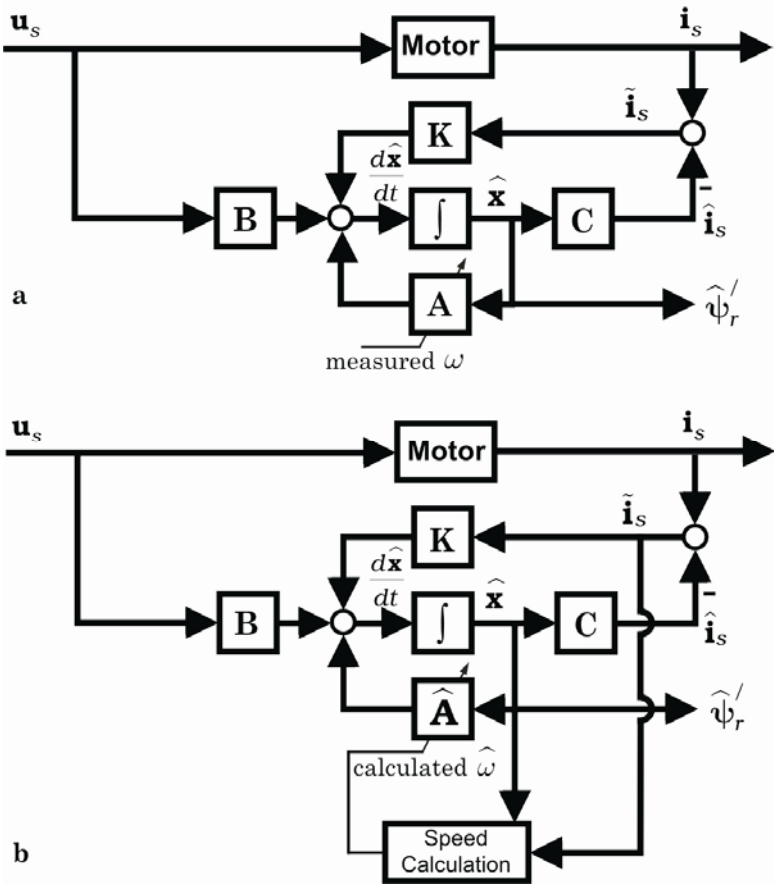

Fig. 4.8 General structure of the rotor flux observer using (**a**) measured and (**b**) estimated speed

There $\tilde{i}_{s\alpha} = i_{s\alpha} - \hat{i}_{s\alpha}$; $\tilde{i}_{s\beta} = i_{s\beta} - \hat{i}_{s\beta}$ are components of the state error vector **e**. The right side of the equation (4.23) contains 3 terms. In order for the system to remain stable, the following conditions must be fulfilled.

1. **K** must be chosen to ensure the negative definiteness of the first term.
2. The estimation algorithm must be designed so that the second and third terms compensate each other, i.e. the sum of the two terms is zero.

In the references [Kubota 1993 and 1994], a frequency dependent correction matrix **K** in the following form is suggested.

$$\mathbf{K} = \left[\begin{array}{cc|cc} k_1 & k_2 & k_3 & k_4 \\ -k_2 & k_1 & -k_4 & k_3 \end{array}\right] \tag{4.24}$$

$$k_1 = -\frac{k-1}{\sigma}\left(\frac{1}{T_r}+\frac{1}{T_s}\right);\ k_2 = (k-1)\hat{\omega};\ k_3 = \frac{k-1}{1-\sigma}\left(\frac{1}{T_r}-\frac{k}{T_s}\right);\ k_4 = \frac{(k-1)\hat{\omega}\sigma}{1-\sigma} \tag{4.25}$$

The idea behind is to fix the poles of the observer (using the constant k>0) proportionally to those of the motor so that the observer (exact like the process or the motor) remains stable. It was found experimentally that k must be chosen in the range of 1 ... 1.5. With this choice the method was tested successfully on different motors, even when only parameterized from name plate data.

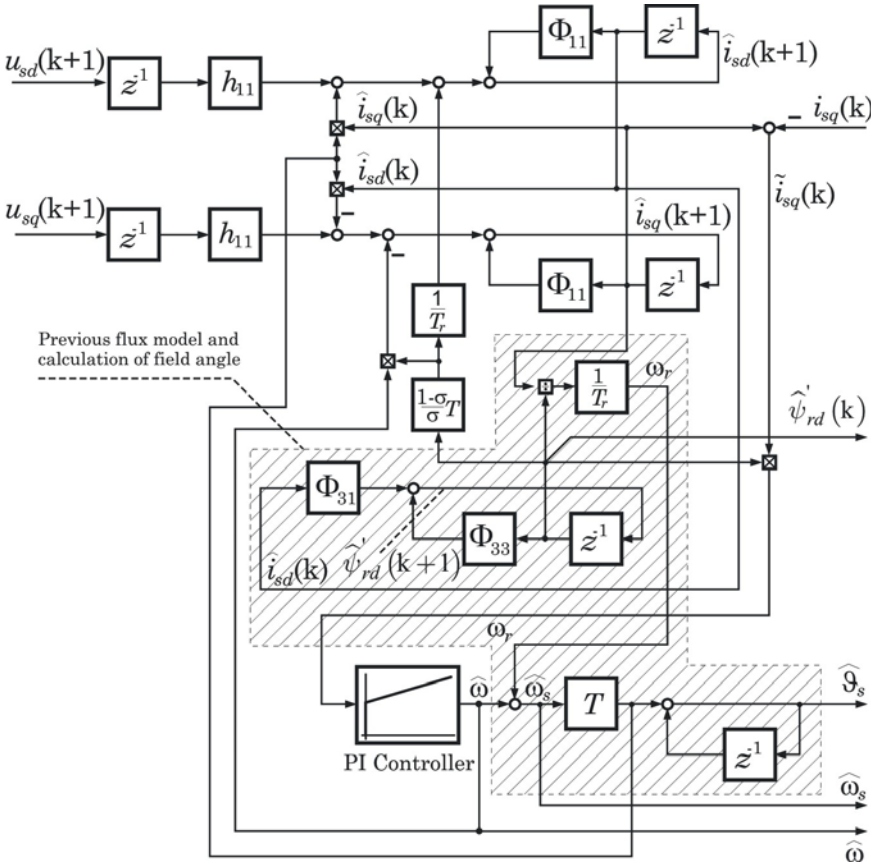

Fig. 4.9 Block circuit diagram of the speed adaptive observer for the calculation of the mechanical angular speed $\hat{\omega}$ and the rotor flux $\hat{\psi}'_{rd}$

In order to fulfil the above second condition concerning the stability, the estimated angular speed $\hat{\omega}$ must fulfill the following equation:

$$\frac{d\hat{\omega}}{dt} = \lambda \frac{1-\sigma}{\sigma} \left(\tilde{i}_{s\alpha} \hat{\psi}'_{r\beta} - \tilde{i}_{s\beta} \hat{\psi}'_{r\alpha} \right) \tag{4.26}$$

Considered that the speed can change fast, equation (4.26) can be augmented to the following PI algorithm to calculate $\hat{\omega}$.

$$\hat{\omega} = K_P e_\omega + K_I \int e_\omega dt \quad \text{with} \quad e_\omega = \tilde{i}_{s\alpha} \hat{\psi}'_{r\beta} - \tilde{i}_{s\beta} \hat{\psi}'_{r\alpha} \tag{4.27}$$

K_P, K_I: Gain factors

For the implementation of the described method the speed error must be transformed into *dq* coordinates first:

$$e_\omega = -\tilde{i}_{sq} \hat{\psi}'_{rd} \quad \text{with} \quad \tilde{i}_{sq} = i_{sq} - \hat{i}_{sq} \tag{4.28}$$

For a step-by-step design we assume first the value $k = 1$ (i.e. flux model without correction). That means, the speed adaptive observer contains the calculation of the current and flux model according to the equation (3.55) (cf. figure 4.7: the hatched area) as well as the PI algorithm (4.27). The angular speed ω_s on the stator side or the stator frequency arises from the following equation:

$$\omega_s = \hat{\omega} + \frac{i_{sq}(k)}{T_r \hat{\psi}'_{rd}(k)} \tag{4.29}$$

The hatched area in figure 4.7 is represented in detail in figure 4.9. The processing of the current control loop is divided into 4 steps (see fig. 4.10, left half), with the estimation algorithm of ω (see fig. 4.9) integrated into the second step, detailed in the right half of the figure 4.10.

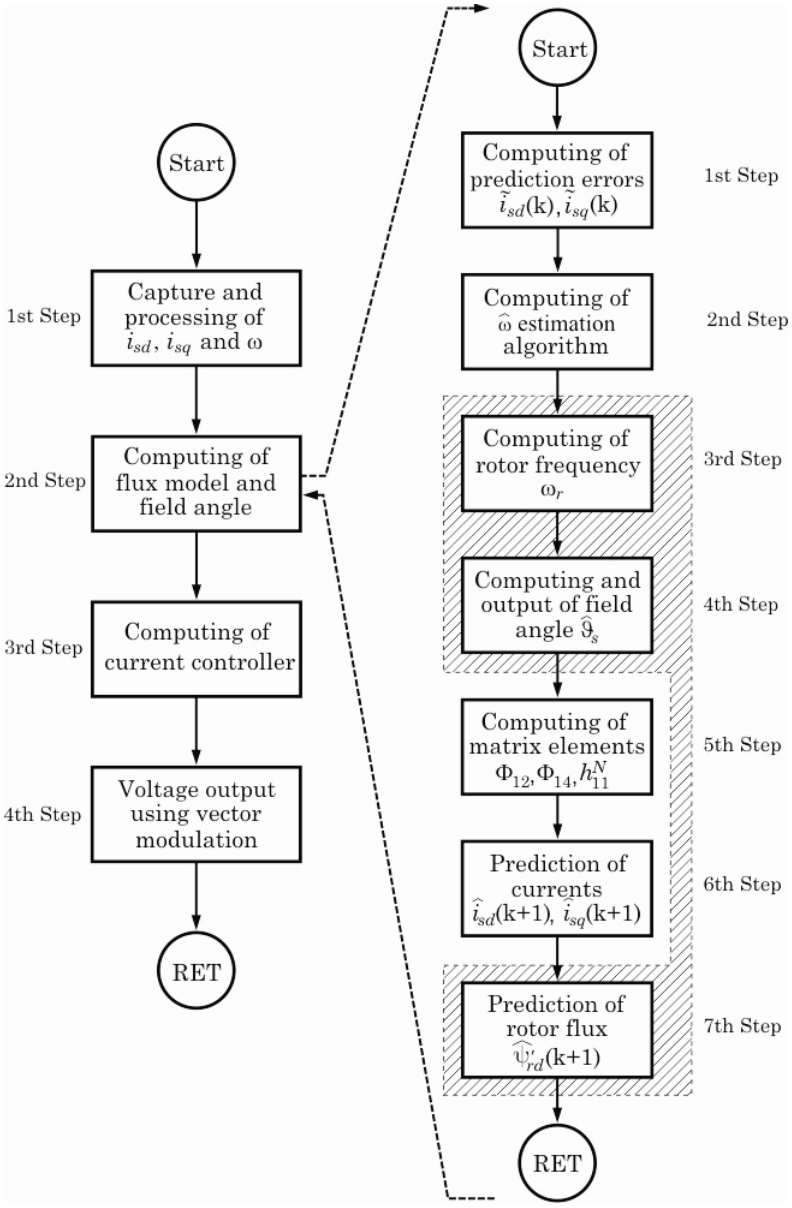

Fig. 4.10 Program flowchart for the implementation of the algorithm from figure 4.9

The speed reversal with field weakening in figure 4.11 illustrates the functionality of the presented method which may be implemented in practical systems easily.

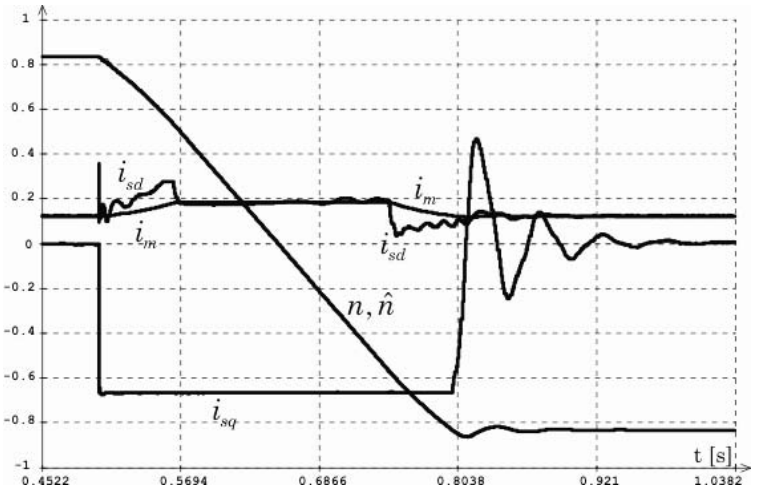

Fig. 4.11 Speed reversal of a sensor-less controlled IM drive: ±3000 min^{-1} with field weakening

The dimensioning of the PI compensation controller (cf. fig. 4.9) is important for the calculation of the speed $\hat{\omega}$. By integrating $\hat{\omega}$ the mechanical angle $\hat{\vartheta}$ is calculated, which forms together with the load angle the transformation angle $\hat{\vartheta}_s$ for the voltage vector output and feedback transformation. I.e. the dynamics of the estimation of ω shows up directly in the innermost loop - the current control loop (cf. figure 4.12). To consider the estimation dynamics in the current controller design, the transfer function $G_e(s)$ is needed.

The transfer function $G_e(s)$ can be derived under the conditions, that:

- the speed in small-signal response only effects the q-axis (cf. 2nd equation from (3.44)), and
- $\psi'_{rd} = \hat{\psi}'_{rd} = i_{sd} = \hat{i}_{sd}$ can be assumed for the d-axis.

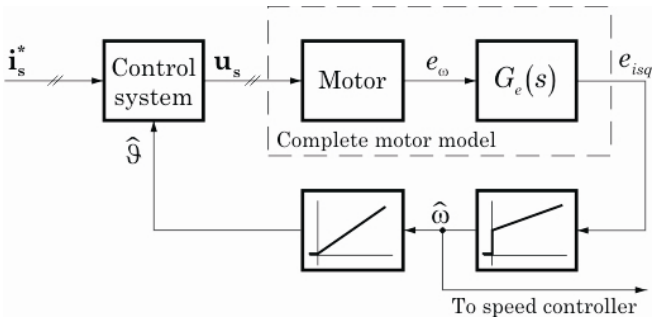

Fig. 4.12 To the necessity of the transfer function $G_e(s)$

Using (3.44) the following equations are obtained in the Laplace domain:

$$\begin{cases} \text{Motor: } s\,i_{sq} = -\omega_s i_{sd} - \dfrac{1}{\sigma}\left(\dfrac{1}{T_s} + \dfrac{1-\sigma}{T_r}\right) i_{sq} - \dfrac{1-\sigma}{\sigma}\omega\psi'_{rd} + \dfrac{1}{\sigma L_s} u_{sq} \\ \text{Model: } s\hat{i}_{sq} = -\hat{\omega}_s \hat{i}_{sd} - \dfrac{1}{\sigma}\left(\dfrac{1}{T_s} + \dfrac{1-\sigma}{T_r}\right) \hat{i}_{sq} - \dfrac{1-\sigma}{\sigma}\hat{\omega}\hat{\psi}'_{rd} + \dfrac{1}{\sigma L_s} u_{sq} \end{cases} \tag{4.30}$$

With

$$e_{isq} = \tilde{i}_{sq} = i_{sq} - \hat{i}_{sq}\,;\; e_\omega = \omega - \hat{\omega}\,;\; \omega_s = \omega + \frac{i_{sq}}{T_r\,\psi'_{rd}}\,;\; \hat{\omega}_s = \hat{\omega} + \frac{\hat{i}_{sq}}{T_r\,\hat{\psi}'_{rd}}$$

from the subtraction of the two equations in (4.30) and after some remodelling we obtain:

$$\frac{e_{isq}(s)}{e_\omega(s)} = \frac{V_e}{1 + s\,T_e} \quad \text{with} \quad T_e = \frac{\sigma\,T_s\,T_r}{T_s + T_r}\,;\; V_e = -\frac{\psi'_{rd}\,T_e}{\sigma} \tag{4.31}$$

K_P, K_I should be chosen to essentially compensate the delay from (4.31) for the closed control loop.

4.3.2 Example for the speed sensor-less control of a PMSM drive

As already mentioned at the beginning of chapter 4.3, two questions must be solved for the speed sensor-less and field orientated operation of a PMSM drive: the *identification of the initial position of the rotor or of the pole flux* and the integration of a *method for the speed sensor-less control*.

The most known publications about the identification of the initial position deal with the case of salient pole machines, where the difference between the direct and the quadrature stator inductance – measured in the *d*- and *q*-axis – is relatively large. This makes a relatively simple off-line identification of the rotor position possible either by an indirect measurement of the inductances or by an evaluation of the currents caused by scanning of the total rotor surface with identical voltage transients. Thanks to new magnet materials with a very high energy density and improved construction techniques the magnets of modern machines are finer distributed and fastened on the rotor surface. However, this improvement with respect to the drive quality aggravates the chance to identify the pole flux position. An interesting approach to solve these

difficulties with moderate processor power has been presented by [Brunotte 1997].

The PMSM is different from the IM physically only by the way of the magnetization: In the IM $\mathbf{i}_m$ or ψ_r' must be built up, whereas the pole flux is permanently available in the PMSM. Therefore it can be assumed, that the Ljapunov stability approach which led to the error model (4.28) for the IM can be used here as well with the speed error signal:

$$e_\omega = -\tilde{i}_{sq}\frac{\psi_p}{L_{sd}} \quad \text{with} \quad \tilde{i}_{sq} = i_{sq} - \hat{i}_{sq} \tag{4.32}$$

As in the case of the asynchronous drive the current error in the *q*-axis is used as an input signal for the ω - PI - estimation controller. Because of the preferred axis of the rotor flux, an error signal for the position angle which helps to eliminate the position error from the beginning must be found. The following considerations help to find a solution. From (3.64) the following equations can be obtained:

$$\begin{cases} \text{Motor:} \quad s\,i_{sd} = -\dfrac{1}{T_{sd}} i_{sd} + s\vartheta_s \dfrac{L_{sq}}{L_{sd}} i_{sq} + \dfrac{1}{L_{sd}} u_{sd} \\ \text{Model:} \quad s\,\hat{i}_{sd} = -\dfrac{1}{T_{sd}} \hat{i}_{sd} + s\hat{\vartheta}_s \dfrac{L_{sq}}{L_{sd}} \hat{i}_{sq} + \dfrac{1}{L_{sd}} u_{sd} \end{cases} \tag{4.33}$$

After the subtraction of the two above equations and some rewriting the following linear relation arises, under the assumption that the ω - transients have died out and the load is constant:

$$\frac{e_{isd}(s)}{e_\vartheta(s)} = \frac{s T_{sq}\, i_{sq}}{1 + s T_{sd}} \tag{4.34}$$

The fault model (4.34) means, that the current error in the *d*- axis can be used as a correction signal for the rotor position. A compensation controller with I behavior, whose output quantity is added to the flux angle, will suffice for this purpose. The figure 4.13 shows the speed reversal of a PMSM drive controlled using this method.

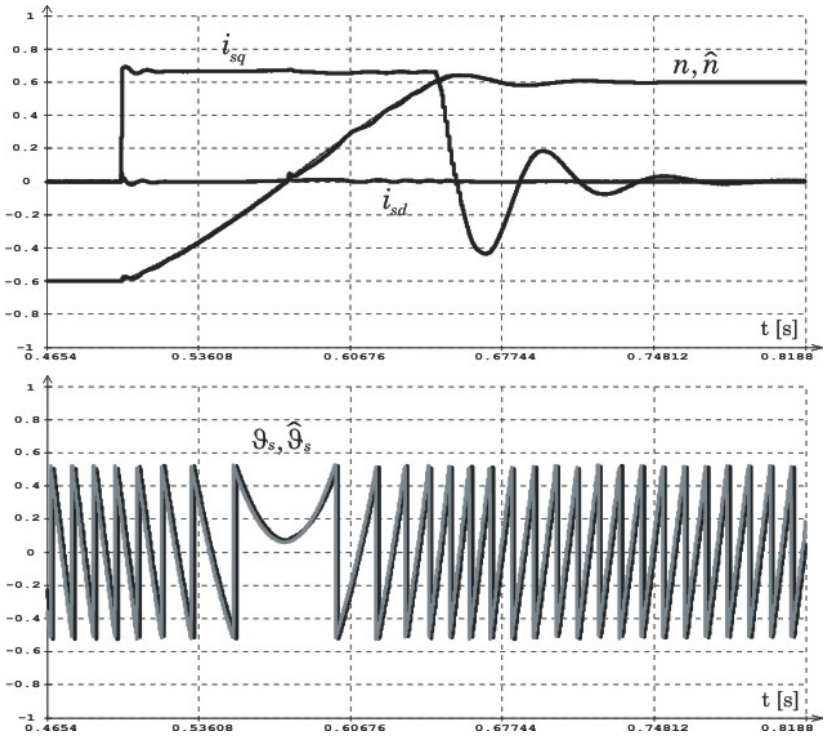

Fig. 4.13 Speed reversal of a speed sensor-less and field-orientated controlled PMSM drive: Currents and speed (**top**), rotor or flux angle (**bottom**)

4.4 Field orientation and its problems

After the essential features of the field-orientated control and important control structures were introduced in chapter 1, some questions of the realization shall be discussed in more detail now. For asynchronous drives the calculation of the rotor flux, which is not measurable without additional costs, is decisive for a successful realization and satisfying control performance. Different models to solve this task will be compared in this chapter. Because control and PWM voltage generation work discontinuously, but the machine, of course, represents a continuous system, a number of issues arise in the context of the interaction of both components. These issues, if disregarded, can have a negative influence on the control accuracy and stability. In the last part of this chapter finally some concrete discretization effects and respective countermeasures will be worked out.

4.4.1 Principle and rotor flux estimation for IM drives

To begin with, some basics of the field orientated control shall be summarized again for the better complete understanding of the matter. As known, the basic idea of the field orientated control is to develop a control structure for the IM similar to that for the DC machine. That means in detail:

1. The process models of torque and flux must be decoupled from each other.
2. At constant flux the torque equation should have a linear characteristic (linear relation between torque and torque-producing quantity).
3. In steady-state, all control variables should be DC quantities.
4. Torque and slip should be proportional. With this proportionality a breakdown-torque caused by the control is avoided, and the maximum torque is expressively determined by the available current or the available voltage.

The requirement 3 is fulfilled by using a reference coordinate system which rotates synchronously with the stator frequency ω_s. The point 2 can be fulfilled, if one axis of the coordinate system is chosen to coincide with the current or the flux vector. It can be shown that under all conceivable variants only the orientation to the vector of the rotor flux (e.g. $\Psi_r = \psi_{rd}$, $\psi_{rq} = 0$) fulfils the remaining requirements and at the same time ensures a dynamically exact decoupling between torque and flux. Stator, rotor voltage and torque equations of the IM (cf. chapter 3 and 6) if splitted into their vector components, then may be rewritten as follows:

$$u_{sd} = R_s i_{sd} + \sigma L_s \frac{\mathrm{d}\, i_{sd}}{\mathrm{d}\, t} - \omega_s \sigma L_s i_{sq} + (1-\sigma) L_s \frac{\mathrm{d}\, i_{md}}{\mathrm{d}\, t} \tag{4.35}$$

$$u_{sq} = R_s i_{sq} + \sigma L_s \frac{\mathrm{d}\, i_{sq}}{\mathrm{d}\, t} + \omega_s \sigma L_s i_{sd} + (1-\sigma) L_s \omega_s i_{md} \tag{4.36}$$

$$0 = i_{md} + T_r \frac{\mathrm{d}\, i_{md}}{\mathrm{d}\, t} - i_{sd} \tag{4.37}$$

$$0 = \omega_r T_r i_{md} - i_{sq} \tag{4.38}$$

$$m_M = \frac{3}{2} z_p \frac{L_m}{L_r} \psi_{rd} i_{sq} = \frac{3}{2} z_p \frac{L_m^2}{L_r} i_{md} i_{sq} = \frac{3}{2} z_p (1-\sigma) L_s i_{md} i_{sq} \tag{4.39}$$

with: $i_{md} = \psi_{rd} / L_m = \psi'_{rd}$

In the context of current impression the very simple signal flowchart in figure 4.14 arises. According to (4.37) and (4.39) the current component i_{sd}

works as a control quantity for the rotor flux, and i_{sq} controls the torque at constant rotor flux.

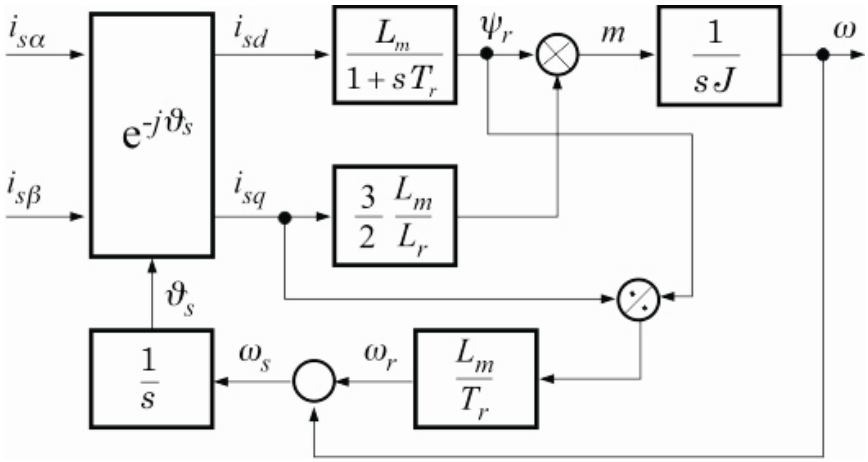

Fig. 4.14 Signal flowchart of the IM in field-orientated coordinates with current impression

Different variants for the implementation of the principle of the rotor flux or field orientation into a control system are conceivable and known. Besides the proposed method using impression of the current vector, all remaining methods differ from each other by their ways to find the modulus and the phase angle of the not directly measurable rotor flux. The exact knowledge of the flux phase angle in stator coordinates

$$\vartheta_s = \arctan\frac{\psi_{r\beta}}{\psi_{r\alpha}} = \vartheta_0 + \int \omega_s \,\mathrm{d}t \tag{4.40}$$

is required for the exact transformation of all measured quantities into field coordinates. Using this angle the current vector in field coordinates is obtained to:

$$\mathbf{i}_s^f = \mathbf{i}_s^s \,\mathrm{e}^{-j\vartheta_s} \tag{4.41}$$

In the simplest case the needed quantities can be calculated with the help of (4.38) from the reference values (set points) of flux and torque (field orientated feed-forward control [Schönfeld 1987] or indirect field orientation [Vas 1994]). A field orientated (feedback) control or a direct orientation uses a direct measuring of, or an estimation model fed by measured motor quantities, for the flux calculation and therefore has the essential advantage that the current motor state can be captured substantially more exact and independent of the quality of the inner current control loop (e.g. at insufficient voltage reserve). Because a direct flux

measuring using Hall sensors or additional coils requires additional incursion in the motor, practically realized systems usually work according to the model method. Typical structures were already introduced and explained in chapter 1.

An analysis of the general voltage equations (ω_k = angular speed of the reference coordinate system)

$$\mathbf{u}_s = R_s\mathbf{i}_s + \sigma L_s \frac{\mathrm{d}\mathbf{i}_s}{\mathrm{d}t} + j\omega_k \sigma L_s \mathbf{i}_s + (1-\sigma)L_s\left(\frac{\mathrm{d}\mathbf{i}_m}{\mathrm{d}t} + j\omega_k \mathbf{i}_m\right) \quad (4.42)$$

$$0 = \left(1 + j(\omega_k - \omega)T_r\right)\mathbf{i}_m + T_r \frac{\mathrm{d}\mathbf{i}_m}{\mathrm{d}t} - \mathbf{i}_s \quad (4.43)$$

shows various possibilities for the calculation or estimation of the rotor flux vector. The different approaches can be distinguished by the used coordinate system and the measured quantities. With regard to the coordinate system characteristically the components of the flux vector are first calculated in stator coordinates, and in the second step modulus and phase angle are derived in field orientated coordinates. Essentially, the following models may be derived (cf. [Verghese 1988], [Zägelein 1984]). Model quantities are indicated with $\hat{}$.

1. u_s - i_s - *Model in stator coordinates*

$$\frac{\mathrm{d}\hat{\mathbf{i}}_m}{\mathrm{d}t} = \frac{\mathbf{u}_s - R_s\mathbf{i}_s}{(1-\sigma)L_s} - \frac{\sigma}{1-\sigma}\frac{\mathrm{d}\mathbf{i}_s}{\mathrm{d}t} \quad (4.44)$$

The model immediately results from the suitable rearrangement of the stator voltage equation. From equation (4.44) it can be noticed that because of the open integration any mechanism for the elimination of state errors, caused by wrong initial values or disturbances, is missing. At low rotational speeds considerable precision problems are to expect because of the significant influence of the stator resistance.

From the rotor voltage equation the following

2. i_s - ω - *Model in stator coordinates*

$$\frac{\mathrm{d}\hat{\mathbf{i}}_m}{\mathrm{d}t} = \left(-\frac{1}{T_r} + j\omega\right)\mathbf{i}_m + \frac{1}{T_r}\mathbf{i}_s \quad (4.45)$$

This model can immediately be derived from the rotor voltage equation. In contrast to (4.44) it can be shown that the state error decays with the rotor time constant [Verghese 1988]. The algorithm contains an integration of sinusoidal input quantities with the corresponding problems at discrete realization, though. This difficulty can be avoided by combination of both models to the following

3. i_s - u_s - ω - *Model in stator coordinates*

The derivation of the flux in (4.42) is eliminated after substituting (4.43):

$$\hat{\mathbf{i}}_m = \frac{-\mathbf{u}_s + (R_s + (1-\sigma)R_r)\mathbf{i}_s + \sigma L_s \frac{\mathrm{d}\mathbf{i}_s}{\mathrm{d}t}}{(1-\sigma)L_s\left(\frac{1}{T_r} + j\omega\right)} \tag{4.46}$$

In equation (4.46) no integration is needed anymore, but three measured quantities are to be fed to the model.

The combination of the first two models to *observers* (exactly: observer of reduced order) allows additionally to influence the system dynamics and with dedicated design also the improvement of the parameter sensitivity [Zägelein 1984].

From the rotor voltage equation in field coordinates the following straightforward

4. i_s - ω - *Model in field coordinates*

$$\frac{\mathrm{d}\,\hat{i}_{md}}{\mathrm{d}\,t} = \frac{1}{T_r}\left(-\hat{i}_{md} + \hat{i}_{sd}\right) \tag{4.47}$$

$$\hat{\vartheta}_s = \hat{\omega}_s = \omega + \frac{\hat{i}_{sq}}{T_r \hat{i}_{md}} \tag{4.48}$$

is obtained. Because the currents here are available only after the coordinate transformation, they also were indicated as model quantities. For this model the comparatively low realization effort can particularly be noticed. Special problems in certain speed ranges do not exist. However, all models derived from the rotor equation have the common property that the precision of the phase angle ϑ_s *strongly depends on the temperature-dependent rotor time constant*.

5. *"Natural Field Orientation" [NFO, Jönsson 1991, 1995]*

Stator frequency and flux phase angle may also be calculated directly from the stator equations. In the NFO approach the calculation is divided between stator and field coordinate system. In stator coordinates the EMF voltage is calculated from equation (4.42):

$$\mathbf{e} = \mathbf{u}_s - R_s\mathbf{i}_s - \sigma L_s \frac{\mathrm{d}\mathbf{i}_s}{\mathrm{d}t} = (1-\sigma)L_s \frac{\mathrm{d}\mathbf{i}_m}{\mathrm{d}t} \tag{4.49}$$

After transformation into field coordinates the stator frequency can be derived from the quadrature component:

$$\omega_s = \frac{e_q}{(1-\sigma)L_s i_{md}} \tag{4.50}$$

In the original method the flux is controlled in open loop, i.e. the reference value is used for i_{md}. However, it is also possible to include a flux control loop for the flux magnitude (4.47) additionally. Neither rotor quantities nor the speed are needed to calculate the phase angle, at least for feed-forward controlled or constant flux. In this respect a close relationship to the u_s - i_s - model in stator coordinates exists. The voltage integration is transferred to an integration of the stator frequency. Similar precision problems at small rotational speeds may be supposed.

So far, the method does not yet contain any speed model. Such an extension is described in [Jönsson 1995], although within a stator flux related control loop.

Finally the possibility of an

6. u_s - ω - *Model*

shall yet be mentioned. To its derivation the currents are eliminated in the voltage and flux equations by mutual substitution, and the stator flux is kept as an auxiliary variable.

In all described models, the rotor magnetizing current i_m was used as an equivalent for the rotor flux magnitude in the first place. The actual rotor flux magnitude would have to be calculated from $\psi_{rd} = L_m\left(\left|\mathbf{i}_\mu\right|\right) i_{md}$ and

$$\left|\mathbf{i}_\mu\right| = \sqrt{\left(\frac{L_{r\sigma}}{L_r} i_{sd} + \frac{L_m}{L_r} i_{md}\right)^2 + \left(\frac{L_{r\sigma}}{L_r} i_{sq}\right)^2} \tag{4.51}$$

Because of the proved positive properties over the whole relevant range of stator frequencies, and because of the simple feasibility, the i_s - ω - model (4.47), (4.48) in field coordinates is often preferred in the practice. Additionally to that, the current measurements are anyway available and high-quality speed controlled drives are equipped with speed measuring facilities.

Consideration of the magnetic saturation is required for high dynamics requirements at operation with variable rotor flux. Corresponding control approaches will be discussed in detail in chapter 6.2. A relatively simple and often satisfactorily used model shall be presented here. For the rotor voltage equation in the arbitrary orientated (rotation frequency ω_κ) *coordinate system* the following equation can be obtained:

$$0 = \mathbf{i}_m - \mathbf{i}_s + \frac{L_m'(|\mathbf{i}_m|) + L_{r\sigma}}{R_r}\frac{\mathrm{d}\,\mathbf{i}_m}{\mathrm{d}\,t} + j\left(\omega_k - \omega\right)\frac{L_m(|\mathbf{i}_m|) + L_{r\sigma}}{R_r}\mathbf{i}_m \tag{4.52}$$

Split into components, the following equations are arrived at

$$\hat{i}_{md} = \hat{i}_{sd} + \frac{\hat{L}_m'(\hat{i}_{md}) + L_{r\sigma}}{R_r}\frac{\mathrm{d}\hat{i}_{md}}{\mathrm{d}t} \tag{4.53}$$

$$\hat{\omega}_s = \hat{\omega}_s = \omega + \frac{\hat{i}_{sq}}{\hat{i}_{md}}\frac{R_r}{L_m(\hat{i}_{md}) + L_{r\sigma}} \tag{4.54}$$

with $L_m'(|\mathbf{i}_\mu|) = \frac{\mathrm{d}|\psi_\mu|}{\mathrm{d}|\mathbf{i}_\mu|} = L_m + \frac{\mathrm{d}L_m}{\mathrm{d}|\mathbf{i}_\mu|}|\mathbf{i}_\mu|$ [1)]

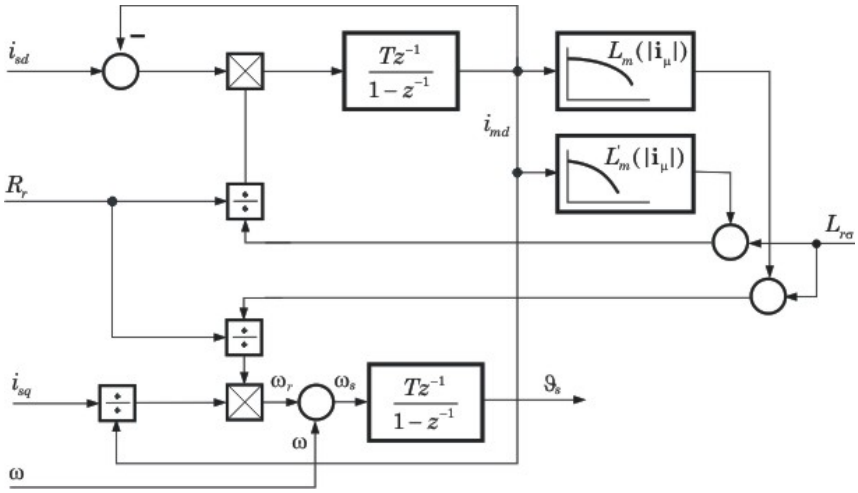

Fig. 4.15 i_s - ω - flux model in field orientated coordinates with saturation of main inductances

Now the i_s - ω - flux model in discrete representation can be rewritten in the following form:

$$\hat{i}_{md}(k+1) = \hat{i}_{md}(k) + \frac{R_r T}{L_m'\left(\hat{i}_{md}(k)\right) + L_{r\sigma}}\left(\hat{i}_{sd}(k) - \hat{i}_{md}(k)\right) \tag{4.55}$$

$$\hat{\vartheta}_s(k+1) = \hat{\vartheta}_s(k) + \omega(k)T + \frac{\hat{i}_{sq}(k)}{\hat{i}_{md}(k)}\frac{R_r T}{L_m\left(\hat{i}_{md}(k)\right) + L_{r\sigma}} \tag{4.56}$$

$$\hat{\vartheta}_s(k+1) = \hat{\vartheta}_s(k) + \hat{\omega}_s(k)T$$

[1)] more about the differential main inductance $L_m'\left(|\mathbf{i}_\mu|\right)$ in chapter 6.2.3

The flux model in this form is represented in figure 4.15. Because of the temperature dependence of the rotor resistance, an on-line tracking of this parameter is additionally required for high-quality drives. The chapter 7 will deal with this problem in greater detail.

4.4.2 Calculation of current set points

Field and torque producing components of the stator current can only be controlled independent of each other as long as the maximum current magnitude is not reached. At this point a suitable strategy for the vectorial current limitation becomes necessary.

The function of the field orientated control relies on the precision or constancy (in the basic speed range) of the impressed rotor flux. Therefore it seems reasonable to give the flux producing component the priority, if the maximum realizable current magnitude is exceeded. A limitation of the maximal reference value i_{sd} to $i_{max}/2$ at the same time allows an adequate control reserve for torque impression. Figure 4.16a illustrates the outlined vector limitation strategy.

If applying a flux control strategy which uses the set point of i_{sq} for calculating the rotor flux set point (cf. chapter 8) an arithmetic loop would arise. This can be avoided by a two-step limitation of i_{sq}^{*} in the speed controller. Figure 4.16b shows the details.

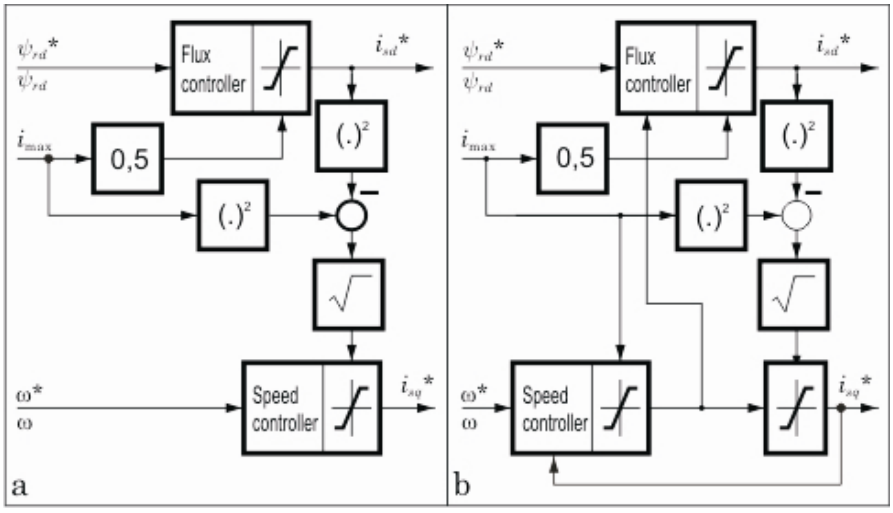

Fig. 4.16 Limitation strategy for calculating the current set points

4.4.3 Problems of the sampling operation of the control system

The problems already discussed in chapter 3.1 for the discretization of the continuous state equations, require a renewed critical assessment at the application within the field orientated control. The system of state equations of the asynchronous machine is the starting point for the design of current controller and flux model, both in field orientated coordinates. In chapter 3.1.2 it was worked out, that for the derivation of an equivalent discrete process model from the continuous state equations the following idealizing prerequisites or approximations must be met:

1. Constancy of the time variant and state-dependent process parameters (frequencies, machine parameters) within a sampling period.
2. Constancy of the input quantities within a sampling period (sampling over zero order hold).

These prerequisites naturally are not fulfilled in the real system, and in the result consequences for precision, control accuracy and stability of a control system, designed on the basis of the mentioned simplifications, have to be expected. Some of these consequences and possible countermeasures shall be examined here. Hereby, we will concentrate on the following main emphases:

1. Validity of the simplifying assumptions for time-variant parameters and input quantities of the continuous system.
2. Choice of the discretization method.
3. Choice of the sampling time.

Thereby the issue (3) must be regarded in closed relation to (1) and (2).

a) Time-variant system parameters

The problem definition can be inverted in a pragmatic way with regard to the time-variant parameters of the system matrix: In order to obtain an equivalent time-discrete system, the boundary conditions of the discretization must be chosen to allow for the system matrix to be considered approximately time-invariant over one sampling period. This primarily has consequences for the selection of the sampling time T which must be chosen adequately small. Time-variant parameters of the system matrix are the speed or mechanical angular velocity ω, the stator angular velocity ω_s and variable (e.g. saturation dependent) machine parameters.

With regard to speed, the prerequisite of approximate time-invariance within a sampling period is fulfilled for usual sampling times of 0.1 ... 1ms. Rotor and stator frequency can change with the dynamics of the impressed torque producing current. The technologically existing limitation of the current allows only a restricted maximum slip and therefore a limited frequency change, though. In the end the assessment of

this point will, however, have to be reserved for the detailed investigation of the concrete application, where stability and performance characteristics have to be investigated. The same is valid for time-variant motor parameters to be taken into account. For the incorporation of the main flux saturation it is advantageous that this quantity also can be seen as depending on a slowly varying state variable (rotor flux).

The input variable of the system is the stator voltage vector $\mathbf{u}_s(t)$. The reference value of $\mathbf{u}_s(t)$ is constant over one sampling period, but for the actual motor voltage this is, however, not the case. For a machine model in stator coordinates the stator voltage is piece-wise constant due to the pulse width modulation, and for a machine model in field coordinates it is piece-wise sinusoidal because of the continuously changing phase angle. Thus the used approximation of zero order will cause errors in every case. A workaround could be the consideration of the actual voltage curve or an approximation of higher order for the calculation of the integral in the output equation (3.9):

$$\mathbf{x}((k+1)T) = \mathrm{e}^{\mathbf{A}T}\,\mathbf{x}(kT) + \int_0^T \mathrm{e}^{\mathbf{A}(T-\tau)}\,\mathbf{B}\mathbf{u}(kT+\tau)\,\mathrm{d}\tau \tag{4.57}$$

(cf. chapter 3.1.2). If the zero-order approximation is retained, it has to be made sure that the mean average value of the model input quantity actually matches the effective mean average value at the machine terminals over a sampling period.

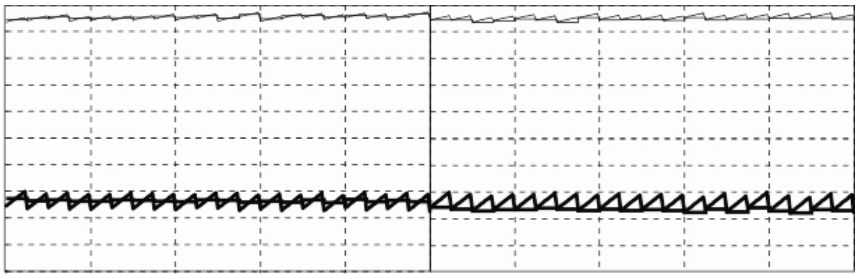

Fig. 4.17 References and actual values of u_{sd} (**bottom**) and u_{sq} (**top**) in field orientated coordinates: with (**left**) and without (**right**) compensation

For a model in field orientated coordinates this can be achieved by a feed-forward compensation of the transformation angle ϑ_s. The equation (4.56) can be amended as follows

$$\hat{\vartheta}_{s1}(k) = \hat{\vartheta}_s(k) + k_c\,\hat{\omega}_s(k)T \tag{4.58}$$

with the new transformation angle ϑ_{s1}. The factor k_c = 1.5 takes additionally into account the dead time of one sampling period between

calculation and output of the control variable. The figure 4.17 shows reference and actual values of the stator voltage in field orientated coordinates with and without the feed-forward compensation of the transformation angle. The pulse width modulation was not simulated in this case.

b) Discretization method

Discretization method and the used approximations decide essentially the stability of the discrete model. This holds particularly when the continuous system matrix contains complex or frequency dependent eigenvalues. To get an opinion about the dimension of the influences and model errors to be expected and also of the differences of the several discretization methods, a series of simulations was carried out whose results are represented in figure 4.18. All parameters of the continuous model are regarded as time-invariant. The state controller with field orientation, described in chapter 5.4, the flux model (4.55), (4.56), (4.58) and a sampling time of T = 0.5ms form the basis of the system under investigation. Because an unstable behavior of the system is recognizable by increasing oscillations, the low-pass filtered norm of the current difference vector of two successive sampling periods was chosen as a performance criterion:

$$Q = \frac{\left\| \mathbf{i}_s(k) - \mathbf{i}_s(k-1) \right\|}{1 + sT_F} \tag{4.59}$$

The criterion was recorded during a speed start-up at maximum acceleration. The following methods were simulated (cf. chapter 3.1.2 and the corresponding example in chapter 12.2):

1. Series expansion of the time-discrete system matrix $\mathbf{\Phi}$ with truncation after the linear term (Euler discretization) (field coordinates).
2. Series expansion of $\mathbf{\Phi}$ with truncation after the quadratic term (field coordinates).
3. Euler discretization in stator coordinates and then transformation into field coordinates.
4. Discretization using substitute function in stator coordinates and subsequent transformation into field coordinates.
5. Discretization using substitute function in field coordinates.
6. Current controller in stator coordinates with integration part and voltage limitation in field coordinates, discretization using substitute function.

For methods 1 - 5 the complete current controller was realized in field coordinates. It shall be emphasized that the simulation did not intend to give any statements about control accuracy, current wave form and the

like, but exclusively aims at the investigation of the control system stability.

The results show significant differences between the methods. It strikes specifically that *a stable operation up to the maximal theoretically possible frequency following the Shannon theorem* can be achieved, *if the method 5 is used*. The method 1 allows a stable operation to just below a stator frequency of 300Hz. This corresponds to the theoretical stability limit of the Euler method with the condition $\left|\lambda_i + 1/T\right| < 1/T$ for the eigenvalues λ_i of the continuous system matrix (cf. chapter 3.1). Since the chosen sampling time rather lies in the upper range of the usually realized values, it is also confirmed that the bigger part of applications – in terms of the implemented control structures – can already be covered with Euler discretization in field orientated coordinates.

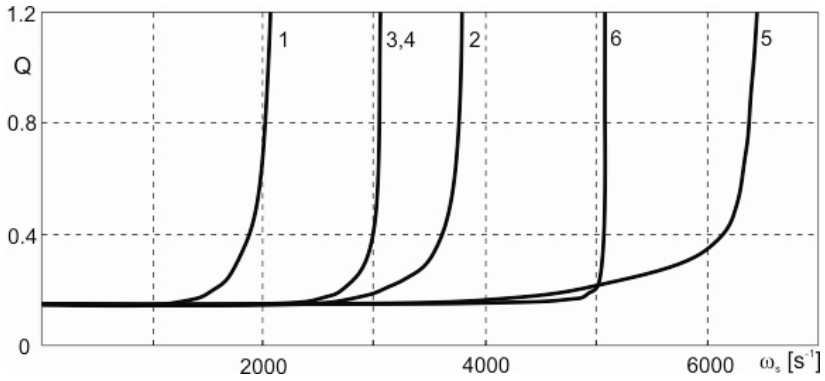

Fig. 4.18 Stability of discretization methods

c) Choice of the sampling time

The choice of the sampling time is one of the most complex problems for the design of a digital control system. To an important part it is a question of the required and available computer power and therefore the hardware costs, in which an optimum is given, because on one hand a minimization of sampling time requires a higher computer power, but on the other hand increasing the sampling time causes the same effect because of the required more sophisticated discretization algorithms.

From the control point of view, stability considerations play a decisive role for the discretization of the continuous model. With regard to the reproducibility of the continuous signals, the absolute lower limit of the sampling frequency is defined by the Shannon theorem. However, for the motor control the opposite case is significant as well: The production of a continuous signal (voltage, current) from a sequence of discrete control

signals (signal reconstruction). For the reconstruction of the continuous signal $f(t)$, using a simple D/A converter (zero order hold), the following maximum amplitude error is obtained, provided steady differentiability of $f(t)$ (cf. [Aström 1984]):

$$e_{A,\max} = \max_k \left| f(k+1) - f(k) \right| \leq T \max_t \frac{\mathrm{d}\, f(t)}{\mathrm{d}\, t} \tag{4.60}$$

For a sinusoidal signal $f(t) = a \sin \omega_s t$ the error results to $e_{A,\max} \leq a\, \omega_s T$. As is easily to comprehend, the maximum amplitude error is reduced for a continuous signal with assumed linear characteristic between two sampling instants and reconstruction by the mean average value, to half of the value for simple sampling at the sampling instants.

Further approaches for the choice of the sampling time can be obtained from the demanded transient response of the closed control system. For a quasi-continuous design, a value of $T \leq (0.25 \ldots 0.5) t_r$ is recommended in [Aström 1984] from the control response time. The relation between sampling and response time is given for the dead-beat design by the system structure. For a small response time the sampling time has to be chosen as small as possible, which however, on other hand, increases the control gain as well as the amplitude of the control variable, and increases the sensitivity to high-frequency disturbances.

The use of fast pulse-width-modulated inverters with constant switching frequency as control equipment yields another influencing factor: Because of the necessary synchronicity between current control and voltage output, the PWM frequency will be chosen as an integer multiple of the sampling frequency of the current control, which yields values in the range of about 0.1 ... 1ms.

4.5 References to chapter 4

Al-Tayie JK, Acarnley PP (1997) Estimation of speed, stator temperature and rotor temperature in cage induction motor drive using the extended Kalman filter algorithm. IEE Proc.-Electr. Power Appl., Vol. 144, No. 5, September, pp. 301 – 309

Aström K, Wittenmark B (1984) Computer Controlled Systems. Prentice-Hall Englewood Cliffs

Beineke S, Grotstollen H (1997) Praxisgerechter Entwurf von Kalman-Filtern für geregelte Synchronmotoren ohne mechanischen Sensor. SPS/IPC/DRIVES 97, Tagungsband, S. 482 – 493

Boyes GS (1980) Synchro and Resolver Conversion. Memory Devices Ltd

Brunotte C, Schumacher W (1997) Detection of the starting rotor angle of a PMSM at standstill. EPE ’97, Trondheim, pp. 1.250 – 1.253

Brunsbach BJ (1991) Sensorloser Betrieb von permanenterregten Synchronmotoren und Asynchronmaschinen mit Kurzschlußläufern durch Zustandsidentifikation. Dissertation, RWTH Aachen

Eulitz Th (1990) Nutzung der Digitalsimulation bei der Entwicklung von Regelstrukturen für Drehstromantriebssysteme. Dissertation, TU Dresden

Isermann R (1988) Identifikation dynamischer Systeme. Bd. II, Springer-Verlag

Jönsson R (1991) Natural Field Orientation for AC Induction Motor Control. PCIM Europe, May/June, pp. 132 – 138

Jönsson R, Leonhard W (1995) Control of an Induction Motor without a Mechanical Sensor, based on the Principle of "Natural Field Orientation" (NFO). International Power Electronics Conference Yokohama

Kiel E (1994) Anwendungsspezifische Schaltkreise in der Drehstrom-Antriebstechnik. Dissertation, TU Carolo - Wilhemina zu Braunschweig

Kubota H, Matsue K, Nakano T (1993) DSP-Based Speed Adaptive Flux Observer of Induction Motor. IEEE Trans. on IA, Vol. 29, No. 2, March/April, pp. 344 – 348

Kubota H, Matsue K (1994) Speed Sensorless Field-Oriented Control of Induction Motor with Rotor Resistance Adaptation. IEEE Trans. on IA, Vol. 30, No. 5, September/October, pp. 1219 – 1224

Matsui N (1996) Sensorless PM Brushless DC Motor Drives. IEEE Trans. on IE, Vol. 43, No. 2, April, pp. 300 – 308

Östlund S, Brokemper M (1996) Sensorless Rotor-Position Detection from Zero to Rated Speed for an Integrated PM Synchronous Motor Drive. IEEE Trans. on IA, Vol. 32, No. 5, September/October

Profumo F, Pastorelli M, Ferraris P, De Doncker RW (1991) Comparision of Universal Field Oriented (UFO) Controllers in Different Reference Frames. Proceedings EPE 1991 Firenze, pp. 689 – 695

Quang NP (1991) Schnelle Drehmomenteinprägung in Drehstromstellantrieben. Dissertation, TU Dresden

Quang NP (1996) Sensorlose feldorientierte Regelung von Asynchronantrieben. Forschungsbericht, TU Dresden

Quang NP, Schönfeld R (1996) Sensorlose und rotorflußorientierte Drehzahl-regelung eines Asynchronantriebs in Feldkoordinaten. SPS/IPC/DRIVES 96, Tagungsband, S. 273 – 282

Rajashekara K, Kawamura A, Matsue K (1996) Sensorless Control of AC Motor Drives: Speed and Position Sensorless Operation. IEEE Press, New York

Saito K (1988) A microprocessor-controlled speed regulator with instantanous speed estimation for motor drive. IEEE Trans. on IE, Vol.35, No.1, Feb., pp. 95 – 99

Schönfeld R (1987) Digitale Regelung elektrischer Antriebe. VEB Verlag Technik Berlin

Stärker K (1988) Sensorloser Betrieb einer umrichtergespeisten Synchron-maschine mittels eines Kalman-Filters. Dissertation, RWTH Aachen

Tajima H, Hori Y (1993) Speed Sensorless Field-Orientation Control of the Induction Machine. IEEE Trans. in IA, Vol. 29, No. 1, January/February

Takeshita T, Matsui N (1996) Sensorless Control and Initial Position Estimation of Salient-Pole Brushless DC Motor. Proc. 4th Intern. Workshop on AMC, Mie University Japan

Texas Instruments (1997) Sensorless Control with Kalman Filter on TMS Fixed-Point DSP. Application Report

Vas P, Drury W (1994) Vector Controlled Drives. Proceedings of PCIM '94 Nürnberg, pp. 213 – 228

Verghese GC, Sanders SR (1988) Observers for Flux Estimation in Induction Machines. IEEE Trans. on Industrial Electronics, Vol. 35, No. 1, Febr., pp. 85 – 94

Zägelein W (1984) Drehzahlregelung des Asynchronmotors unter Verwendung eines Beobachters mit geringer Parameterempfindlichkeit. Dissertation, Universität Erlangen-Nürnberg